Journal Pre-proof

Efficient construction of boron nitride network in epoxy composites combining reaction-induced phase separation and three-roll milling

Cong Gao, Zihao Zhu, Yucai Shen, Tingwei Wang, Dong Xiang

PII: S1359-8368(20)33282-0

DOI: https://doi.org/10.1016/j.compositesb.2020.108232

Reference: JCOMB 108232

To appear in: *Composites Part B*

Received Date: 9 January 2020

Revised Date: 4 June 2020

Accepted Date: 10 June 2020

Please cite this article as: Gao C, Zhu Z, Shen Y, Wang T, Xiang D, Efficient construction of boron nitride network in epoxy composites combining reaction-induced phase separation and three-roll milling, *Composites Part B*, https://doi.org/10.1016/j.compositesb.2020.108232.

Efficient construction of boron nitride network in epoxy composites combining reaction-induced phase separation and three-roll milling

Cong Gao[a], Zihao Zhu[a], Yucai Shen[a*], Tingwei Wang[a], Dong Xiang[b]

[a] College of Materials Science & Engineering, Nanjing Tech University, Nanjing, 211816, China

[b] School of Materials Science and Engineering, Southwest Petroleum University, Chengdu, 610500, China

Corresponding author

e-mail: ycshen@njtech.edu.cn (Yucai Shen)

ABSTRACT

Self-construct of filler network was developed to enhance the thermal conductivity of epoxy based composites. The selective distribution of hexagonal boron nitride (hBN) particles in epoxy/PES blends and enhanced dispersion of hBN were successfully obtained by reaction-induced phase separation (RIPS) and three-roll milling (TRM),

respectively. The agglomeration of hBN particles in epoxy composite was significantly decreased by three-roll milling, and this was also supported by micromechanics theory, resulting in the construction of the highly efficient filler network. Compared with conventional epoxy/hBN composites and epoxy/PES/hBN composites prepared by mechanical stirring, the epoxy/PES/hBN composites fabricated by three-roll milling showed a great enhancement in thermal conduction and impact strength. The thermal conductivities of the epoxy/PES/hBN composites fabricated by three-roll milling reached 0.52 W/mK at a loading of 10 wt% hBN, which is almost 2.6 times that of the neat epoxy, 40.5% and 26.8% higher than that of epoxy/hBN composites and epoxy/PES/hBN composites without three-roll milling, respectively. Furthermore, the micron-size hBN has a greater advantage for thermal transfer in comparison with boron nitride nanosheets (BNNS). This study provides a readily scalable production method which allows for exfoliation of BN fillers as well as in situ construction of filler networks in thermosetting resin with an environmental friendly route.

Key words: Epoxy composites; Boron nitride; Thermal conductivity

1. Introduction

The upgrade and update of electronic components and large electrical equipment have put higher demands on the reliability of thermally conductive and insulating materials [1-3]. Stability and lifetime of energy systems such as solar power and

light-emitting diodes (LEDs) have been significantly affected by thermal and insulating properties of materials [4, 5]. Polymers have received widespread attention because of the wonderful processability and excellent dielectric property (such as epoxy resins), but most polymers exhibit lower thermal transfer capabilities (about 0.1-0.5 W/mK) [6, 7]. Most ceramic fillers have been added to achieve high thermal conductivity and electrical insulation in polymer composites, such as aluminum nitride [8], hexagonal boron nitride [9-12], silicon carbide [13], etc., which have been used for realizing high thermal conductivity enhancement in composites.

Addition of a large amount of fillers to the polymer matrix can greatly enhance the thermal conductive performance of composites. However, high viscosity and deteriorated mechanical property limit the production and processing of composites [14]. The construction of a continuous thermally conductive pathway to improve the utilization of fillers has become an essential issue in the preparation of high thermal conductivity composites [15, 16]. One method is to build a three-dimensional interconnect filler network to obtain high thermal conductive composites at a low filler loading [17]. However, complicated processes of the method have limited applications in large-scale fabrication. Another approach is to construct segregated architecture, fillers with high thermal conductivity are located at the interfaces of polymer granules, forming a dense thermal conductive network by hot pressing [18]. The application in the commercial field is still limited in spite of the simple compression molding process, and it only fits for thermoplastic polymer composites. The selective distribution of fillers

could also form continuous thermal conductive paths in two immiscible polymer blends [19]. The strategy has received more attention in thermoplastic/thermoplastic systems, which also been applied in electrically conductive composites [20]. In the thermoplastic/thermosetting resin system, thermal conductive network can be designed by reaction-induced phase separation (RIPS), and phase structure of final blends is mainly related to the content of thermoplastic matrix [21]. A suitable phase structure of polymer blends could be formed to function as a carrier for fillers to construct a continuous filler network structure, which could achieve thermal conductive paths at low filler loading. However, the efficiency of the formation of filler network still need to be improved.

Hexagonal boron nitride (hBN) has a wide band gap (5-6eV), which makes it have high electrical resistivity and low dielectric constant [22]. It also has a high thermal conductivity [23]. The lattice structure of a hBN monolayer is similar to graphene，and the properties of composites may be affected owing to the stacking and agglomeration of hBN particles [24]. A small amount of boron nitride flakes can be obtained by sonication in water or organic solvent [25], but the low yield of hBN flakes and high cost of organic solvents have limited the application in mass production. In addition, the functionalization of hBN reduces the interaction between the layers, which can obtain a certain amount of few-layer hBN [26]. With the aid of molten hydroxide, the insertion of cations (Na^+ or K^+) and anions (OH^-) increases the self-curling energy of the hBN sheet，and it can also obtain the boron nitride nanosheet [27]. Another approach is

exfoliation with a shear force, such as ball milling [28], or using a vortex fluidic device (VFD), the shear action from gravity and centrifugal force could exfoliate hBN particles [29]. However, the complicated processes and low yields have limited the mass production in commercial applications.

In this work, the hBN particles were used as thermally conductive filler and in situ exfoliated by three-roll milling, and thus reduce the adverse effects of stacking and agglomeration of hBN particles in the polymer blend. In addition, polyethersulphone (PES) was introduced into epoxy system, leading to construct an efficient filler interconnect network through reaction-induced phase separation. With different hBN content, the influence of three-roll milling on various properties of the composites has been discussed. Compared with the samples prepared by mechanical stirring, three-roll milling has improved the dispersion of hBN particles in the blend and enhanced the thermal conductive property and impact performance of the filled composites. For comparison, boron nitride nanosheet (BNNS) was also used in this system. Compared with the micro-size hexagonal boron nitride (hBN), BNNS has no obvious advantages for the enhancement of thermal conductivity.

2. Experimental

2.1 Materials

Hexagonal boron nitride (hBN) (diameter: 15-25 μm) was purchased from Dandong Rijin Technology Co. Ltd. (China). Boron nitride nanosheet (BNNS)

(thickness: 50-400 nm) was suppiled by Nanjing Xianfeng Nano Material Technology Co. Ltd. Epoxy oligomers were diglycidyl ethers of bisphenol A supplied from Nantong Xingchen Material Co. Ltd., China. Polyethersulphone (PES) with Mn around 6.7×10^4 was purchased from Jilin University, China. Methyl tetrahydrophthalic anhydride (MTHPA) as the curing agent was supplied from Zhejiang Alpha Technology Co. Ltd., China. The curing accelerator was 2-ethyl-4-methylimidazole, provided by Sinopharm Group, China.

2.2 Preparation of epoxy composites

PES powder was added and dissolved in liquid curing agent MTHPA at 110 ^{o}C for 2 h. Epoxy oligomers were added in the mixture (PES : MTHPA : epoxy = 3 : 8 : 10, by mass ratio), and then mechanical stirred in an oil bath at 90 ^{o}C for 20 min. The hBN with different mass fractions (from 1 wt% to 10 wt% of the blends) was mixed in the blends and stirred for 20 min. The blends were then fed into the three-roll mill. After passing through three-roll milling for five times at room temperature, the blends were cast in mold and cured at 145 ^{o}C for 4 h. The schematic diagram of the preparation process of epoxy composites is shown in Fig. 1. Samples prepared by three-roll milling were named as epoxy/PES/hBN-TRM, and samples with the name of epoxy/PES/hBN were fabricated by mechanical stirring without three-roll milling. Epoxy/hBN composites were prepared as the contrast samples. Epoxy and hBN particles were mixed by mechanical stirring at 90 ^{o}C for 20 min. To reduce the precipitation of hBN particles

in the epoxy/BN mixture, the composites were precured at 100 ^{o}C for 1 h and postcured at 145 ^{o}C for another 4 h.

2.5. Characterization

The contact angle was measured by a drop shape analysis system (DSA100, KRUSS). Film samples of hBN and PES were fabricated through hot pressing, while a thin layer of epoxy oligomer was applied to the surface of glass slide [30]. The measurements were performed with water (H_2O) and diiodomethane (CH_2I_2) as probe liquid at room temperature. The images of scanning electron microscope (Jeol JSM-6510, Japan) and optical microscope (Carl Zeiss Jena, Germany) were obtained on the section of the samples to investigate the morphology of the composites. The thermal conductivity of samples with thickness of 8 mm was tested using Hot Disk Thermal Analyzer (TPS 2500) at room temperature. An infrared thermograph (FOTRIC 220) was used to obtain the thermal images of the composites. Un-notched impact property was measured by an Izod impact tester (UJ-4, Chengde Machine, China). The frequency dependent electrical conductivity and dielectric performance of the composites were measured by a broadband dielectric spectrometer (Novocontrol technologies, Concept 42) from 0.1 Hz to 1 MHz at room temperature.

3. Results and discussion

3.1. Theoretical prediction of hBN location

For two incompatible polymer blend systems, the distribution of fillers is affected by interactions between the different componets [20]. Therefore, the distribution of hBN in the blends can be predicted by the affinity to the certain polymer. The interactions between hBN and other polymer matrix can be evaluated be the wetting parameter (ω_a), which is widely used to predict the location of fillers in blends [31]. The value of ω_a for different components can be calculated by Eq. (1):

$$\omega_a = \frac{\gamma_{\text{hBN-B}} - \gamma_{\text{hBN-A}}}{\gamma_{\text{A-B}}} \quad (1)$$

where $\gamma_{\text{hBN-A}}$ and $\gamma_{\text{hBN-B}}$ are the interfacial tensions between hBN fillers and polymer A and B, respectively, while $\gamma_{\text{A-B}}$ is the interfacial tension between polymer A and polymer B. If $\omega_a > 1$, the hBN particles are present in polymer A; if $\omega_a < -1$, the hBN particles distribute in polymer B; and if $-1 < \omega_a < 1$, the hBN particles are located at the interface between the two polymers. The interfacial tension between two components can be calculated using the harmonic mean equation and the geometric mean equation [32].

Harmonic mean equation:

$$\gamma_{12} = \gamma_1 + \gamma_2 - 4\left(\frac{\gamma_1^d \gamma_2^d}{\gamma_1^d + \gamma_2^d} + \frac{\gamma_1^p \gamma_2^p}{\gamma_1^p + \gamma_2^p}\right) \quad (2)$$

Geometric mean equation:

$$\gamma_{12} = \gamma_1 + \gamma_2 - 2\sqrt{\gamma_1^d \gamma_2^d} - 2\sqrt{\gamma_1^p \gamma_2^p} \quad (3)$$

where γ_i is the surface tensions of components i, $\gamma_i = \gamma_i^d + \gamma_i^p$; γ_i^d is the dispersive part of the surface tension of components i; and γ_i^p is the polar part of the surface tension of components i. Surface tension, dispersive and polar portion of the polymer and hBN can be evaluated from the contact angle of the component in H_2O and CH_2I_2. The relationship between the contact angle θ and the surface tension γ_i is as follows [33]:

$$\gamma_L(1+\mathrm{COS}\theta) = 2\sqrt{\gamma_S^d\gamma_L^d} + 2\sqrt{\gamma_S^p\gamma_L^p} \quad (4)$$

where γ_L and γ_S are the surface tension of the liquid and solid, γ_L^d and γ_L^p are the dispersive and polar portions of liquid, γ_S^d and γ_S^p are the dispersive and polar portions of solid. The surface energies of components and interfacial tension between materials are listed in Table 1 and Table 2.

The wetting parameters (ω_a) for the studied epoxy composites were calculated and shown in Table 3. The calculated value of ω_a indicated that hBN particles preferred to distribute in PES phase or the junction of epoxy and PES.

3.2. Morphologies of the epoxy/PES/hBN-TRM composites

The elemental content of epoxy/PES/hBN composites fabricated by mechanical stirring with 10 wt% hBN was shown in Fig. S1. It can be seen that the smooth fractured surface was epoxy phase, and the network-like phase (area 1) was PES phase where a large amount of boron and nitrogen elements were found. This indicated the selective distribution of hBN particles in the polymer blends.

The SEM images of hBN particles and epoxy/PES/hBN composites fabricated by three-roll milling are shown in Fig. 2. From the Fig. 2(A), hBN particles exhibited smooth lamellar structure and the particle size was between 15 and 20 μm, with thickness around 1μm. Fig. 2(B-F) show the SEM images of cryo-fractured surface of epoxy/PES/hBN composites by three-roll milling with different contents of hBN. It is clear that the PES phase is continuous, while the hBN particles were selectively dispersed in the PES phase. With the increasing content of hBN, a filler network tended to form. The SEM images of morphologies of epoxy/hBN composites and epoxy/PES/hBN composites prepared by different strategies are shown in Fig. 3. Fig. 3(A) illustrates the cryo-fractured surface of epoxy/hBN composite. It can be seen that the distribution of hBN in the epoxy matrix was random. In Fig. 3(B) and (C), hBN was dispersed in the PES phase which had the potential to form a continuous heat conduction path. However, there were agglomerations in epoxy/hBN composites and epoxy/PES/hBN composites prepared by mechanical stirring, which was exhibited in Fig. 3(a) and (b). Fig. 3(c) presents that there were no obvious agglomeration in epoxy/PES/hBN composite by three-roll milling with 10 wt% hBN. The SEM images of epoxy/PES composites with 5 wt% loading of BNNS are shown in Fig. S2. It can be found that the agglomerations of BNNS were appeared in epoxy/PES/hBN composites prepared by mechanical stirring. The detailed discussion is shown in supporting information.

The optical microscope images of epoxy/PES/hBN-TRM composites with different

content of hBN are shown in Fig. 4 to investigate the distribution and dispersion of hBN in large scale. The light area was the continuous phase of PES, while the dark area was the dispersed phase of epoxy, and the hBN particles (shown by arrows) are dispersed in PES or the phase interface. The difference of epoxy phase between epoxy/PES/hBN and epoxy/PES/hBN-TRM composites is shown in Fig.S3. At low contents of fillers, no continuous thermal conductive path was formed (Fig. 4(A-C)), and with the increasing of fillers, the filler networks were gradually formed (Fig. 4(D) and (F)). The optical microscope images of epoxy/hBN composites and epoxy/PES/hBN composites are shown in Fig. 5. In low and high magnification, significant agglomeration was observed in epoxy/hBN composites and epoxy/PES/hBN composites fabricated by mechanical stirring (Fig. 5(A), (B), (a) and (b)), while no significant agglomeration was observed for epoxy/PES/hBN-TRM composites and highly efficient filler network has formed. This is consistent with the SEM results, indicating that the three-roll milling process is greatly effective in reducing the agglomeration of hBN particles, leading to a highly efficient way to form a filler network.

3.3. Thermal performance of epoxy/PES/hBN-TRM composites

The thermal conductive properties of epoxy/hBN and epoxy/PES/hBN composites system prepared by different strategies are illustrated in Fig. 6(a). With the increasing filling amount of hBN particles, the thermal conductivities of epoxy/hBN composites increased linearly. At low filler loadings (1-5 wt%), the thermal conductivties of

epoxy/PES/hBN composites were close to that of epoxy/hBN composites. However, the epoxy/PES/hBN composites exhibited enhanced thermal conductivity in comparison with epoxy/hBN composites at 7 wt% hBN loading. It can be inferred that 7 wt% hBN content was a critical value, and at low filler loading, there are insufficient hBN to construct a three-dimension continuous filler network. In addition, the epoxy/PES/hBN composite fabricated by three-roll milling exhibited significantly higher thermal conductive performance even at a low hBN loading of 3 wt%. The thermal conductivity of epoxy/PES/hBN-TRM composites with 10 wt% hBN was 0.52 W/mK, which was 160% and 40.5% improvement compared with pure epoxy and epoxy/hBN composites, respectively, and 26.8% higher than that of epoxy/PES/hBN composites without three-roll milling. The thermal conductivity of epoxy/PES composites filled with hBN and BNNS is shown in Table S1. It can be seen that the thermal conductivity of epoxy/PES/BNNS composites has not been significantly improved. Furthermore, the comparative values of thermal conductivity with previously reported epoxy composites are shown in Table 4 [2, 11, 34-41]. In this work, the enhancement in the epoxy/PES/hBN-TRM composites is due to the deagglomeration of hBN by three-roll milling combined with the following selective distribution of hBN via reaction-induced phase separation. As a result, a highly efficient thermal conductive pathway can be formed in the epoxy matrix, as illustrated in Fig. 7.

Furthermore, theoretical model was also applied to relate the thermally conductive behavior of composites with the dispersion of fillers. According to the micromechanics

theory [42, 43], the effective thermal conductivity K_c can be calculated using the following formula:

$$\frac{K_c}{K_m} = \frac{f}{3}\left[\frac{1}{H + (K_x / K_m - 1)^{-1}} + \frac{2}{(1-H)/2 + (K_z / K_m - 1)^{-1}}\right] + 1 \quad (5)$$

where K_m (0.2 W/mK) means the thermal conductivity of the polymer matrix, f represents the volume fraction of the hBN, K_x and K_z represent the in-plane and out-of-plane thermal conductivities of the hBN. Herein, values of K_x and K_z were assumed 200 W/mK and 150 W/mK [44, 45], respectively. H is the geometrical factor related to the aspect ratio, p = L / d, and calculated as follows:

$$H_p = \frac{1}{p^2 - 1}\left[\frac{p}{\sqrt{p^2 - 1}} \ln(p + \sqrt{p^2 - 1}) - 1\right] \quad (6)$$

Fig. S3 shows the influence of aspect ratio p on thermal conductivities of composites predicted by Eq. (5). The relationship between mass fraction and volume fraction was shown in Eq. (S5). From the Fig. 6b, it can be seen that the experimental data has a good agreement with the modelling data, implying that aspect ratios of hBN played a significant role in the thermal conduction. It can be clearly seen that the simulated results of the thermal conductivity of epoxy/PES/hBN-TRM composites agrees well with the experimental data when the aspect ratio was 14 for the model. This value of 14 was much higher than that of epoxy/hBN composite (aspect ratio of 9) and epoxy/PES/hBN composite (aspect ratio of 9~11), which means that three-roll milling could increase the average aspect ratio of hBN in the epoxy composites by improving

the dispersion of hBN particles. Interestingly, the aspect ratio of a single hBN particle used in this work was around 15~20 as can be calculated from Fig. 2(A). The epoxy/PES/hBN-TRM composites exhibited significant enhancement in thermal conductivity even at 3 wt% content of hBN, compared with epoxy/PES/hBN composites without three-roll milling. This could be due to the improved dispersion of hBN by three-roll milling allowing hBN particles to efficiently form a thermal conductive network at a lower filler loading. This was consistent with the experimental data.

The increased thermal transport properties of epoxy/PES/hBN-TRM composites are clearly illustrated by infrared thermographs. Fig. 8(a) shows the temperature distribution images of neat epoxy and epoxy composites at 0, 60 and 120 s. The color of epoxy/PES/hBN-TRM composites with 10 wt% hBN loading changed quickly from black to orange, which indicated that the epoxy/PES/hBN-TRM composites illustrated higher thermal transfer efficiency due to the efficient thermal conductive network built by three-roll milling. The temperature-time curve of four samples is shown in Fig. 8(b). This exhibits that epoxy/PES/hBN-TRM composites have higher heating rates than that of pure epoxy and other composites. After heating for 300 s, the temperature of the epoxy/PES/hBN-TRM composites with 10 wt% hBN loading was 14.1 ^{o}C higher than that of pure epoxy, which illustrated that epoxy/PES/hBN-TRM composites showed good potential in thermal management.

3.4. Impact performance of epoxy/PES/hBN-TRM composites

Fig. 9 shows the impact performance of epoxy/PES/hBN composites prepared by different methods. All epoxy/PES/hBN-TRM composites had significantly higher impact strength compared with the epoxy/PES/hBN composites by mechanical stirring. This may be due to the agglomeration of hBN becoming a stress concentration point, and three-roll milling improved the dispersion of hBN in the PES phase and enhances the impact strength of the composites [46, 47].

3.5. Dielectric properties of epoxy/PES/hBN-TRM composites

The dependence on frequency of the dielectric constant and loss for pure epoxy and epoxy composites is shown in Fig. 10. The low dielectric constant and dielectric loss are very important for applications in electrical devices packaging. Owing to the high dielectric constant of hBN, the epoxy composites showed high dielectric constants in comparison with the pure epoxy. However, the difference was not significant, which indicated that the effect of hBN on the dielectric constant was negligible. At medium and high frequencies (10 Hz to 1 MHz), the dielectric loss tangent of all composites was close to that of pure epoxy. At low frequencies (0.1 Hz to 10 Hz), the dielectric loss of epoxy/hBN composites and epoxy/PES/hBN composites exhibited a slightly higher than that of pure epoxy. The dielectric loss tangent was closely related to electrical conductivity [48, 49]. The increased dielectric loss tangent of epoxy composites at low frequencies may be attributed to an addition of the electrical conductivity, which was

confirmed in Fig. 10(c). It can be seen that the conductivity of the samples was around 10^{-14} S/cm at 1 Hz, which proved that the composites had great electrical insulation [50]. Furthermore, the epoxy/PES/hBN composite prepared by three-roll milling had lower dielectric loss and electrical conductivity at low frequencies than that fabricated without three-roll milling. This could be caused by the addition of hBN which can inhibit the migration of carriers. The uniformly dispersed hBN increased interfaces between fillers and polymer matrix, leading to a reduction in dielectric loss [49]. Accordingly, the epoxy/PES/hBN composites prepared by TRM had good prospects in practical applications.

4. Conclusions

The selective dispersion of hBN particles in epoxy/PES blends was obtained by RIPS, which formed a three-dimensional interconnected conductive network structure. Epoxy/PES/hBN composites exhibited great enhancement of thermal conductivity and improved impact strength compared with epoxy/hBN composites. Moreover, the SEM images and OM images showed that TRM improved the dispersion of hBN in epoxy/PES composites. The theoretical prediction based on the micromechanics theory indicated that the improved dispersion can be attributed to the increasing of the aspect ratio by three-roll milling. The comparison between hBN and BNNS shows that the nanofillers have no obvious advantages for the enhancement of thermal conductivity.

Therefore, the three-dimensional filler network could be efficiently developed at a lower content of hBN particles. Furthermore, the addition of hBN did not significantly increase the dielectric constant and loss of the epoxy composites. Consequently, efficient filler network can be constructed combining reaction-induced phase separation and three-roll milling, leading to the enhanced thermal, mechanical and dielectric performance of epoxy composites.

Acknowledgments

We acknowledge National Natural Science Foundation of China (51703096) for the funding, and the Priority Academic Program Development of Jiangsu Higher Education Institutions (PAPD) for the support.

References

[1] Losego MD, Grady ME, Sottos NR, Cahill DG, Braun PV. Effects of chemical bonding on heat transport across interfaces. Nat Mater 2012;11(6):502-6.

[2] Doan VC, Vu MC, Thieu NAT, Islam MA, Park PJ, Kim SR. Copper flake-coated cellulose scaffold to construct segregated network for enhancing thermal conductivity of epoxy composites. Compos Part B-Eng 2019;165:772-8.

[3] Guo Y, Lyu Z, Yang X, Lu Y, Ruan K, Wu Y, et al. Enhanced thermal conductivities and decreased thermal resistances of functionalized boron nitride/polyimide composites. Compos Part B-Eng 2019;164:732-9.

[4] Cho E, Huang J, Li C, Chang-Jian C, Lee K, Hsiao Y. Graphene-based thermoplastic composites and their application for LED thermal management. Carbon 2016;102:66-73.

[5] Wang M, Lin S. Anisotropic and Ultralow Phonon Thermal Transport in Organic-Inorganic Hybrid Perovskites: Atomistic Insights into Solar Cell Thermal Management and Thermoelectric Energy Conversion Efficiency. Adv Funct Mater 2016;26(29):5297-306.

[6] Ram R, Soni V, Khastgir D. Electrical and thermal conductivity of polyvinylidene fluoride (PVDF) - Conducting Carbon Black (CCB) composites: Validation of various theoretical models. Compos Part B-Eng 2020;185:107748.

[7] Chen H, Ginzburg VV, Yang J, Yang Y, Liu W, Huang Y. Thermal conductivity of polymer-based composites: Fundamentals and applications. Prog Polym Sci 2016;59:41-85.

[8] Dang TML, Kim C, Zhang Y, Yang J, Masaki T, Yoon D. Enhanced thermal conductivity of polymer composites via hybrid fillers of anisotropic aluminum nitride whiskers and isotropic spheres. Compos Part B-Eng 2017;114:237-46.

[9] Pan C, Kou K, Zhang Y, Li Z, Wu G. Enhanced through-plane thermal conductivity of

PTFE composites with hybrid fillers of hexagonal boron nitride platelets and aluminum nitride particles. Compos Part B-Eng 2018;153:1-8.

[10] Guo Y, Lyu Z, Yang X, Lu Y, Ruan K, Wu Y, Kong J, Gu J. Enhanced thermal conductivities and decreased thermal resistances of functionalized boron nitride/polyimide composites. Compos Part B-Eng 2019;164:732-9.

[11] Yang X, Zhu J, Yang D, Zhang J, Guo YQ, Gu J. High-efficiency improvement of thermal conductivities for epoxy composites from synthesized liquid crystal epoxy followed by doping BN fillers. Compos Part B-Eng 2020;185:107784.

[12] Yang X, Guo Y, Han Y, Li Y, Ma TB, Chen MJ, Kong J, Zhu JH, Gu J. Significant improvement of thermal conductivities for BNNS/PVA composite films via electrospinning followed by hot-pressing technology. Compos Part B-Eng 2019;175:107070.

[13] Xiao C, Guo Y, Tang Y, Ding JW, Zhang X, Zheng K, Tian XY. Epoxy composite with significantly improved thermal conductivity by constructing a vertically aligned three-dimensional network of silicon carbide nanowires/boron nitride nanosheets. Compos Part B-Eng 2020;187:107855.

[14] Chen C, Tang Y, Ye YS, Xue Z, Xue Y, Xie X. High-performance epoxy/silica coated silver nanowire composites as underfill material for electronic packaging. Compos Sci Technol 2014;105:80-5.

[15] Guo S, Zheng R, Jiang J, Yu JH, Dai K, Yan C. Enhanced thermal conductivity and retained electrical insulation of heat spreader by incorporating alumina-deposited graphene filler in nano-fibrillated cellulose. Compos Part B-Eng 2019;178:107489.

[16] Zhang X, Maira B, Hashimoto Y, Wada T, Chammingkwan P, Thakur A. Selective localization of aluminum oxide at interface and its effect on thermal conductivity in polypropylene/polyolefin elastomer blends. Compos Part B-Eng 2019;162:662-70.

[17] Ji C, Yan C, Wang Y, Xiong SX, Zhou FR, Li YY, Sun R. Thermal conductivity enhancement of CNT/MoS2/graphene-epoxy nanocomposites based on structural synergistic effects and interpenetrating network. Compos Part B-Eng 2019;163:363-70.

[18] Zhou H, Deng H, Zhang L, Fu Q. Significant Enhancement of Thermal Conductivity in Polymer Composite via Constructing Macroscopic Segregated Filler Networks. ACS Appl Mater Interfaces 2017;9(34):29071-81.

[19] Yorifuji D, Ando S. Enhanced thermal conductivity over percolation threshold in polyimide blend films containing ZnO nano-pyramidal particles: advantage of vertical double percolation structure. J Mater Chem 2011;21(12):4402.

[20] Göldel A, Marmur A, Kasaliwal GR, Pötschke P, Heinrich G. Shape-Dependent Localization of Carbon Nanotubes and Carbon Black in an Immiscible Polymer Blend during Melt Mixing. Macromolecules 2011;44(15):6094-102.

[21] Deng H, Lin L, Ji M, Zhang S, Yang M, Fu Q. Progress on the morphological control

of conductive network in conductive polymer composites and the use as electroactive multifunctional materials. Prog Polym Sci 2014;39(4):627-55.

[22] Golberg D, Bando Y, Huang Y, Terao T, Mitome M, Tang C. Boron Nitride Nanotubes and Nanosheets. ACS Nano 2010;4(6):2979-93.

[23] Jo I, Pettes MT, Kim J, Watanabe K, Taniguchi T, Yao Z. Thermal Conductivity and Phonon Transport in Suspended Few-Layer Hexagonal Boron Nitride. Nano Lett 2013;13(2):550-4.

[24] Warner JH, Rümmeli MH, Bachmatiuk A, Büchner B. Atomic Resolution Imaging and Topography of Boron Nitride Sheets Produced by Chemical Exfoliation. ACS Nano 2010;4(3):1299-304.

[25] Coleman JN, Lotya M, O'Neill A, Bergin SD, King PJ, Khan U, et al. Two-dimensional nanosheets produced by liquid exfoliation of layered materials. Science 2011;331(6017):568-71.

[26] Lei W, Mochalin VN, Liu D, Qin S, Gogotsi Y, Chen Y. Boron nitride colloidal solutions, ultralight aerogels and freestanding membranes through one-step exfoliation and functionalization. Nat Commun 2015;6(1):8849.

[27] Li X, Hao X, Zhao M, Wu Y, Yang J, Tian Y. Exfoliation of Hexagonal Boron Nitride by Molten Hydroxides. Adv Mater 2013;25(15):2200-4.

[28] Lee D, Lee B, Park KH, Ryu HJ, Jeon S, Hong SH. Scalable Exfoliation Process for

Highly Soluble Boron Nitride Nanoplatelets by Hydroxide-Assisted Ball Milling. Nano Lett 2015;15(2):1238-44.

[29] Chen X, Dobson JF, Raston CL. Vortex fluidic exfoliation of graphite and boron nitride. Chem commun 2012;48(31):3703.

[30] Abbasian A, Ghaffarian SR, Mohammadi N, Fallahi D. The contact angle of thin-uncured epoxy films: thickness effect. Colloid Surface A 2004;236(1-3):133-40.

[31] Sumita M, Sakata K, Asai S, Miyasaka K, Nakagawa H. Dispersion of fillers and the electrical conductivity of polymer blends filled with carbon black. Polym Bull 1991;25(2):265-71.

[32] Baudouin A, Devaux J, Bailly C. Localization of carbon nanotubes at the interface in blends of polyamide and ethylene–acrylate copolymer. Polymer 2010;51(6): 1341-54.

[33] Owens DK, Wendt RC. Estimation of the surface free energy of polymers. J Appl Polym Sci 1969;13(8):1741–7.

[34] Xiao C, Chen L, Tang Y, Zhang X, Zheng K, Tian X. Enhanced thermal conductivity of silicon carbide nanowires (SiCw)/epoxy resin composite with segregated structure. Compos Part A-Appl Sci Manuf 2019;116:98-105.

[35] Han Y, Shi X, Yang X, Guo Y, Zhang J, Kong J. Enhanced thermal conductivities of epoxy nanocomposites via incorporating in-situ fabricated hetero-structured SiC-BNNS

fillers. Compos Sci Technol 2020;187:107944.

[36] Jiang Y, Shi X, Feng Y, Li S, Zhou X, Xie X. Enhanced thermal conductivity and ideal dielectric properties of epoxy composites containing polymer modified hexagonal boron nitride. Compos Part A-Appl Sci Manuf 2018;107:657-64.

[37] Yang X, Fan S, Li Y, Guo Y, Li Y, Ruan K. Synchronously improved electromagnetic interference shielding and thermal conductivity for epoxy nanocomposites by constructing 3D copper nanowires/thermally annealed graphene aerogel framework. Compos Part A-Appl Sci Manuf 2020;128:105670.

[38] Ren L, Li Q, Lu J, Zeng X, Sun R, Wu J. Enhanced thermal conductivity for Ag-deposited alumina sphere/epoxy resin composites through manipulating interfacial thermal resistance. Compos Part A-Appl Sci Manuf 2018;107:561-9.

[39] Zhou H, Wang H, Du X, Mo Y, Yuan H, Liu H. Hybrid three-dimensional graphene fillers and graphite platelets to improve the thermal conductivity and wear performance of epoxy composites. Compos Part A-Appl Sci Manuf 2019;123:270-7.

[40] Oh H, Kim K, Ryu S, Kim J. Enhancement of thermal conductivity of polymethyl methacrylate-coated graphene/epoxy composites using admicellar polymerization with different ionic surfactants. Compos Part A-Appl Sci Manuf 2019;116:206-15.

[41] Wang L, Qiu H, Liang C, Song P, Han Y, Han Y. Electromagnetic interference shielding MWCNT-Fe3O4@Ag/epoxy nanocomposites with satisfactory thermal

conductivity and high thermal stability. Carbon 2019;141:506-14.

[42] Chu K, Jia C, Li W. Effective thermal conductivity of graphene-based composites. Appl Phys Lett 2012;101(12):121916.

[43] Deng F, Zheng Q, Wang L, Nan C. Effects of anisotropy, aspect ratio, and nonstraightness of carbon nanotubes on thermal conductivity of carbon nanotube composites. Appl Phys Lett 2007;90(2):21914.

[44] Chang C W, Fennimore A M, Afanasiev A, et al. Isotope effect on the thermal conductivity of boron nitride nanotubes. Phys Rev Lett 2006;97(8):85901.

[45] Jo I, Pettes M T, Kim J, et al. Thermal Conductivity and Phonon Transport in Suspended Few-Layer Hexagonal Boron Nitride. Nano Lett 2013;13(2):550-554.

[46] Jyotishkumar P, Logakis E, George SM, Pionteck J, Häussler L, Haßler R. Preparation and properties of multiwalled carbon nanotube/epoxy-amine composites. J Appl Polym Sci 2013;127(4):3063-73.

[47] Yang X, Tang L, Guo Y, Liang C, Zhang Q, Kou K. Improvement of thermal conductivities for PPS dielectric nanocomposites via incorporating NH_2-POSS functionalized nBN fillers. Compos Part A-Appl Sci Manuf 2017;101:237-42.

[48] Tanaka T. Dielectric nanocomposites with insulating properties. IEEE Trans Dielectr Electr Insul 2005;12(5):914-28.

[49] Huang X, Zhi C, Jiang P, Golberg D, Bando Y, Tanaka T. Polyhedral Oligosilsesquioxane-Modified Boron Nitride Nanotube Based Epoxy Nanocomposites: An Ideal Dielectric Material with High Thermal Conductivity. Adv Funct Mater 2013;23(14):1824-31.

[50] Zou D, Huang X, Zhu Y, Chen J, Jiang P. Boron nitride nanosheets endow the traditional dielectric polymer composites with advanced thermal management capability. Compos Sci Technol 2019;177:88-95.

Figures captions:

Fig. 1. Schematic illustration of epoxy/PES/hBN composites prepared by three-roll milling.

Fig. 2. SEM images of (A) BN particles; (B) epoxy/PES/hBN composites by three-roll milling with 1 wt% hBN; (C) 3 wt% hBN; (D) 5 wt% hBN; (E) 7 wt% hBN; (F) 10 wt% hBN.

Fig. 3. SEM images of (A) epoxy/hBN composite by mechanical stirring with 10 wt% hBN; (B) epoxy/PES/hBN composite by mechanical stirring with 10 wt% hBN; (C) epoxy/PES/hBN composite by three-roll milling with 10 wt% hBN; (a), (b) and (c) corresponding to high magnification.

Fig. 4. Optical microscope images of epoxy/PES/hBN-TRM composites at different

hBN contents: (A) 1 wt%; (B) 3wt %; (C) 5 wt%; (D) 7 wt%; (E) 10 wt%.

Fig. 5. Optical microscope images of (A) epoxy/10%hBN composites; (B) epoxy/PES/10%hBN composites; (C) epoxy/PES/10%hBN composites by three-roll milling; (a), (b) and (c) corresponding to high magnification.

Fig. 6. (a) Thermal conductivities of epoxy/hBN, epoxy/PES/hBN and epoxy/PES/hBN-TRM composites with different contents of hBN; (b) The experimental and predicted thermal conductivity of epoxy/hBN composites and epoxy/PES/hBN composites fabricated by different methods.

Fig. 7. Schematic representation of epoxy composites prepared via RIPS with three-roll milling.

Fig. 8. Thermal images (a) and temperature-time curve (b) of (□) pure epoxy; (□) epoxy/hBN, (□) epoxy/PES/hBN and (□) epoxy/PES/hBN-TRM composites with 10 wt% hBN loading.

Fig. 9. Impact strength of epoxy/PES/hBN composites fabricated by different methods.

Fig. 10. Frequency dependent dielectric constant (a), dielectric loss tangent (b) and electrical conductivity (c) of pure epoxy; epoxy/hBN, epoxy/PES/hBN and epoxy/PES/hBN-TRM composites with 10 wt% hBN loading.

Table 1 The surface energy data of components.

Table 2 Interfacial tensions γ_{12} between different components calculated using the harmonic and geometric mean equation.

Table 3 Wetting parameter as calculated using the harmonic and geometric mean equation.

Table 4 Comparison of epoxy-based composites with different fillers.

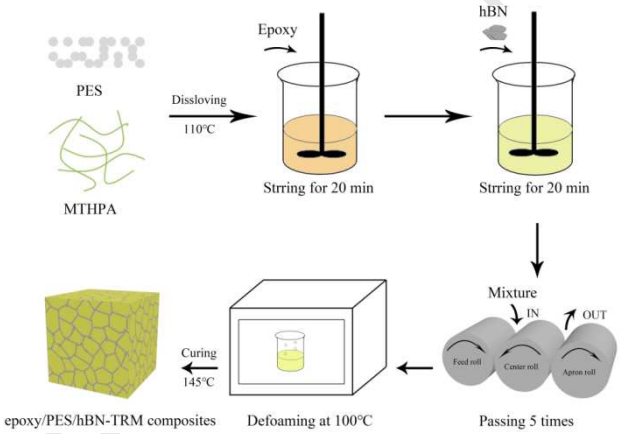

Fig. 1

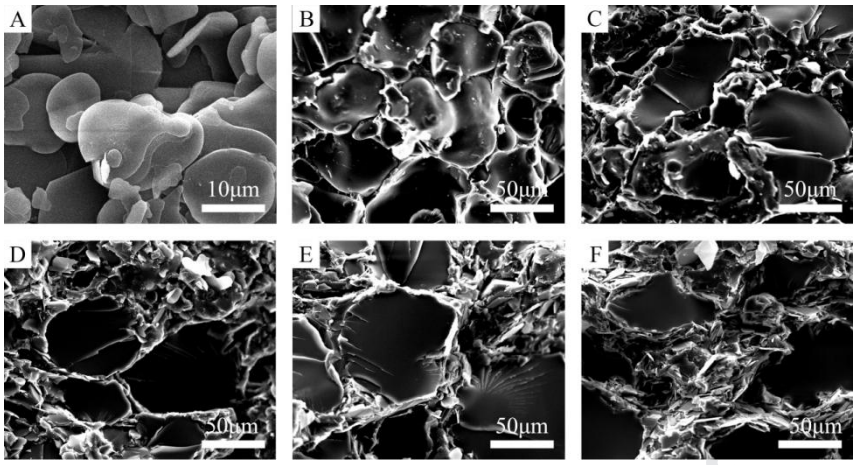
A
10μm
B
50μm
C
50μm
D
50μm
E
50μm
F
50μm

Fig. 2

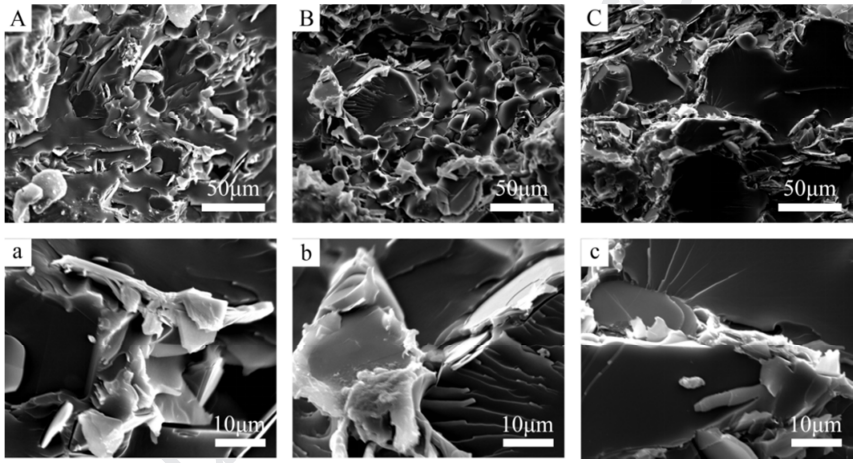
A
50μm
B
50μm
C
50μm
a
10μm
b
10μm
c
10μm

Fig. 3

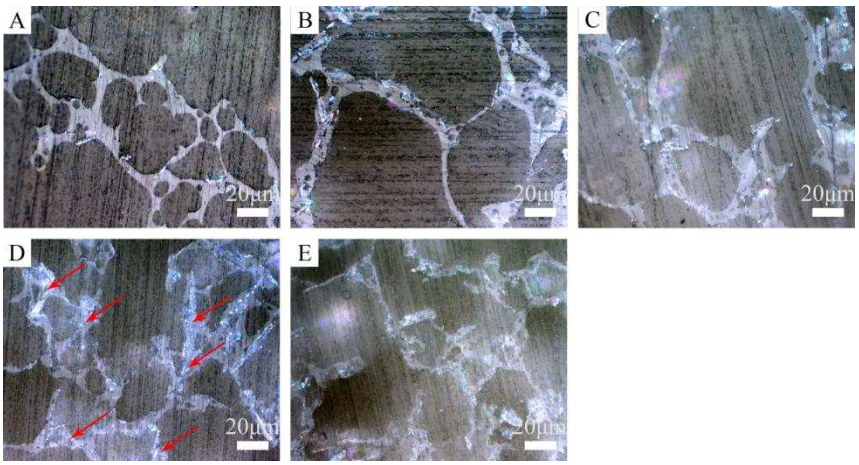
A
20μm
B
20μm
C
20μm
D
20μm
E
20μm

Fig. 4

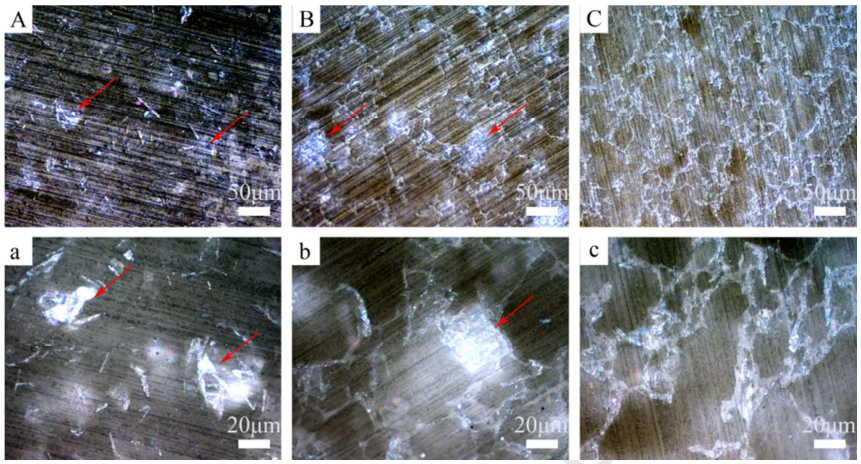

Fig. 5

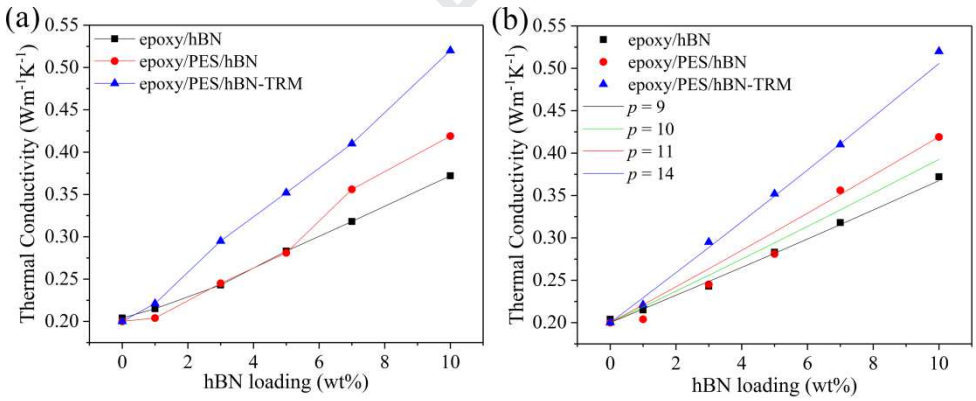

Fig. 6

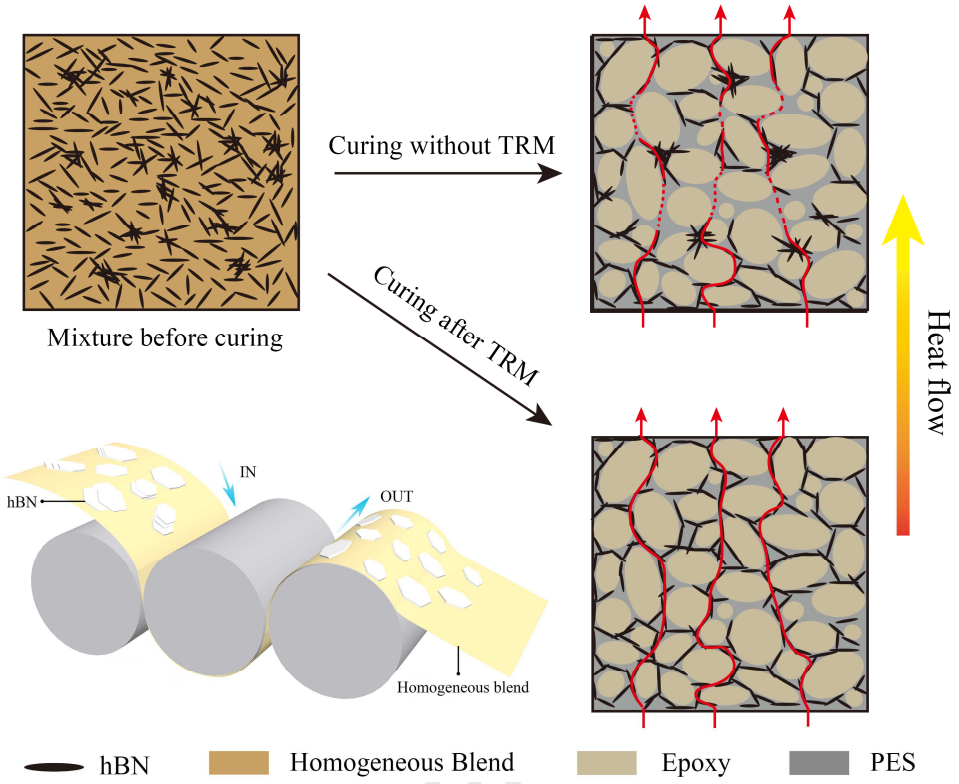
Curing without TRM
Curing after TRM
Mixture before curing
Heat flow
IN
OUT
hBN
Homogeneous blend
hBN
Homogeneous Blend
Epoxy
PES

Fig. 7

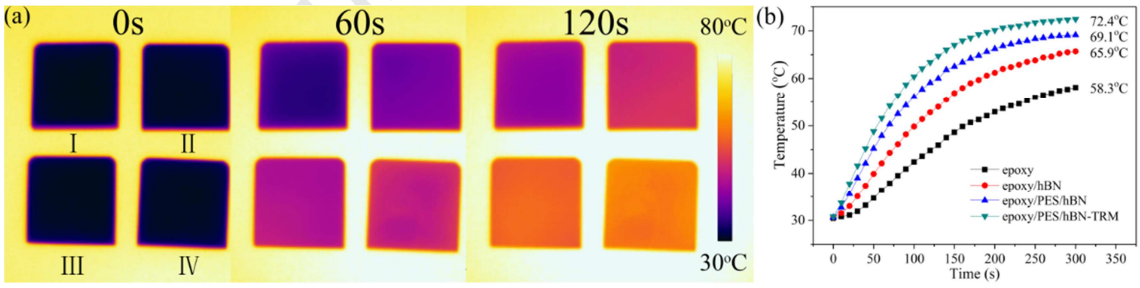
(a)
0s
60s
120s
80°C
30°C
I
II
III
IV
(b)
Temperature (°C)
Time (s)
72.4°C
69.1°C
65.9°C
58.3°C
epoxy
epoxy/hBN
epoxy/PES/hBN
epoxy/PES/hBN-TRM

Fig. 8

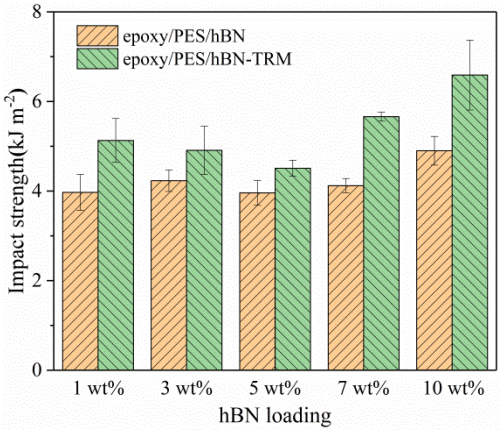

Fig. 9

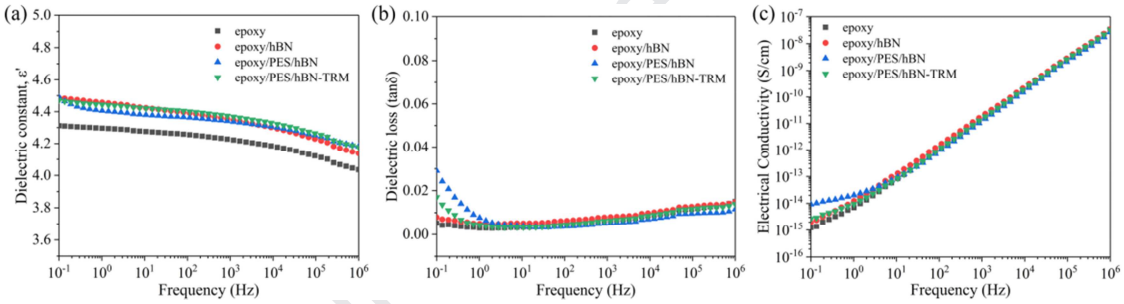

Fig. 10

Components	γ^d (mN m^{-1})	γ^p (mN m^{-1})	γ (mN m^{-1})
PES	27.9	9.8	37.7

Epoxy	38.5	13.7	52.2
hBN	41.8	0.7	42.5

Table 1

Component couple	γ_{12} (mN m^{-1})	
	Harmonic mean equation	Geometric mean equation
PES-hBN	10.74	6.75
Epoxy-hBN	11.95	8.37
Epoxy-PES	2.64	1.48

Table 2

Sample	ω_a (Harmonic mean equation)	ω_a (Geometric mean equation)
Epoxy/PES/hBN	-0.46	-1.10

Table 3

Composites	Filler content	Thermal conductivity (W/mK)	Complexity of processing	Test method	Year & References
epoxy/*f*-SiC_w	3.91 vol%	0.43	Medium	Hot disk	2019 [34]
epoxy/(SiC + BNNS)	20 wt%	0.89	Medium	Hot disk	2020 [35]
LCER/BN	30 wt%	1.02	Medium	Hot disk	2020 [11]
epoxy/BN-PGMA	15 vol%	1.198	Medium	Hot disk	2018 [36]
epoxy/CuNWs-TAGA	7.2 wt%	0.51	High	Hot disk	2020 [37]
epoxy/Al_2O_3-AgNPs	70 wt%	1.304	Medium	Laser flash	2018 [38]
epoxy/Cu@Cell	36.4 wt%	1.4	Medium	Laser flash	2019 [2]
epoxy/(3DGF + GP)	5.52 vol%	0.68	High	Laser flash	2019 [39]
epoxy/c-PfRG	3 wt%	0.67	High	Laser flash	2019 [40]
epoxy/(MWCNT + Fe_3O_4@Ag)	15 wt%	0.46	High	Laser flash	2019 [41]
epoxy/PES/BN	10 wt%	0.52	Low	Hot disk	This work

Table 4

Notes:

f-SiC_w: modified silicon carbide nanowires;

BNNS: boron nitride nanosheets;

LCER: liquid crystal epoxy resin;

BN-PGMA: BN grafted by poly (glycidylmethacrylate);

CuNWs-TAGA: 3D CuNWs-thermally annealed graphene aerogel;

Al_2O_3-AgNPs: silver nanoparticle-decorated Al_2O_3 spheres;

Cu@Cell: cellulose-supported copper scaffold;

3DGF: 3D graphene fillers; GP: graphite platelets;

c-PfRG: polymethylmethacrylate-functionalized graphenes using cetyltrimethylammonium bromide.

MWCNT: multiwall carbon nanotube.

Table 1 The surface energy data of components.

Components	γ^d (mN m^{-1})	γ^p (mN m^{-1})	γ (mN m^{-1})
PES	27.9	9.8	37.7
Epoxy	38.5	13.7	52.2
hBN	41.8	0.7	42.5

Table 2 Interfacial tensions γ_{12} between different components calculated using the harmonic and geometric mean equation.

Component couple	γ_{12} (mN m^{-1})	
	Harmonic mean equation	Geometric mean equation
PES-hBN	10.74	6.75
Epoxy-hBN	11.95	8.37
Epoxy-PES	2.64	1.48

Table 3 Wetting parameter as calculated using the harmonic and geometric mean equation.

Sample	ω_a (Harmonic mean equation)	ω_a (Geometric mean equation)
Epoxy/PES/hBN	-0.46	-1.10

Table 4 Comparsion of epoxy-based composites with different fillers.

Composites	Filler content	Thermal conductivity (W/mK)	Complexity of processing	Test method	Year & References
epoxy/*f*-SiC_w	3.91 vol%	0.43	Medium	Hot disk	2019 [34]
epoxy/(SiC + BNNS)	20 wt%	0.89	Medium	Hot disk	2020 [35]
LCER/BN	30 wt%	1.02	Medium	Hot disk	2020 [11]
epoxy/BN-PGMA	15 vol%	1.198	Medium	Hot disk	2018 [36]
epoxy/CuNWs-TAGA	7.2 wt%	0.51	High	Hot disk	2020 [37]
epoxy/Al_2O_3-AgNPs	70 wt%	1.304	Medium	Laser flash	2018 [38]
epoxy/Cu@Cell	36.4 wt%	1.4	Medium	Laser flash	2019 [2]
epoxy/(3DGF + GP)	5.52 vol%	0.68	High	Laser flash	2019 [39]
epoxy/c-PfRG	3 wt%	0.67	High	Laser flash	2019 [40]
epoxy/(MWCNT + Fe_3O_4@Ag)	15 wt%	0.46	High	Laser flash	2019 [41]
epoxy/PES/BN	10 wt%	0.52	Low	Hot disk	This work

Notes:

f-SiC_w: modified silicon carbide nanowires;

BNNS: boron nitride nanosheets;

LCER: liquid crystal epoxy resin;

BN-PGMA: BN grafted by poly (glycidylmethacrylate);

CuNWs-TAGA: 3D CuNWs-thermally annealed graphene aerogel;

Al_2O_3-AgNPs: silver nanoparticle-decorated Al_2O_3 spheres;

Cu@Cell: cellulose-supported copper scaffold;

3DGF: 3D graphene fillers; GP: graphite platelets;

c-PfRG: polymethylmethacrylate-functionalized graphenes using cetyltrimethylammonium bromide.

MWCNT: multiwall carbon nanotube.

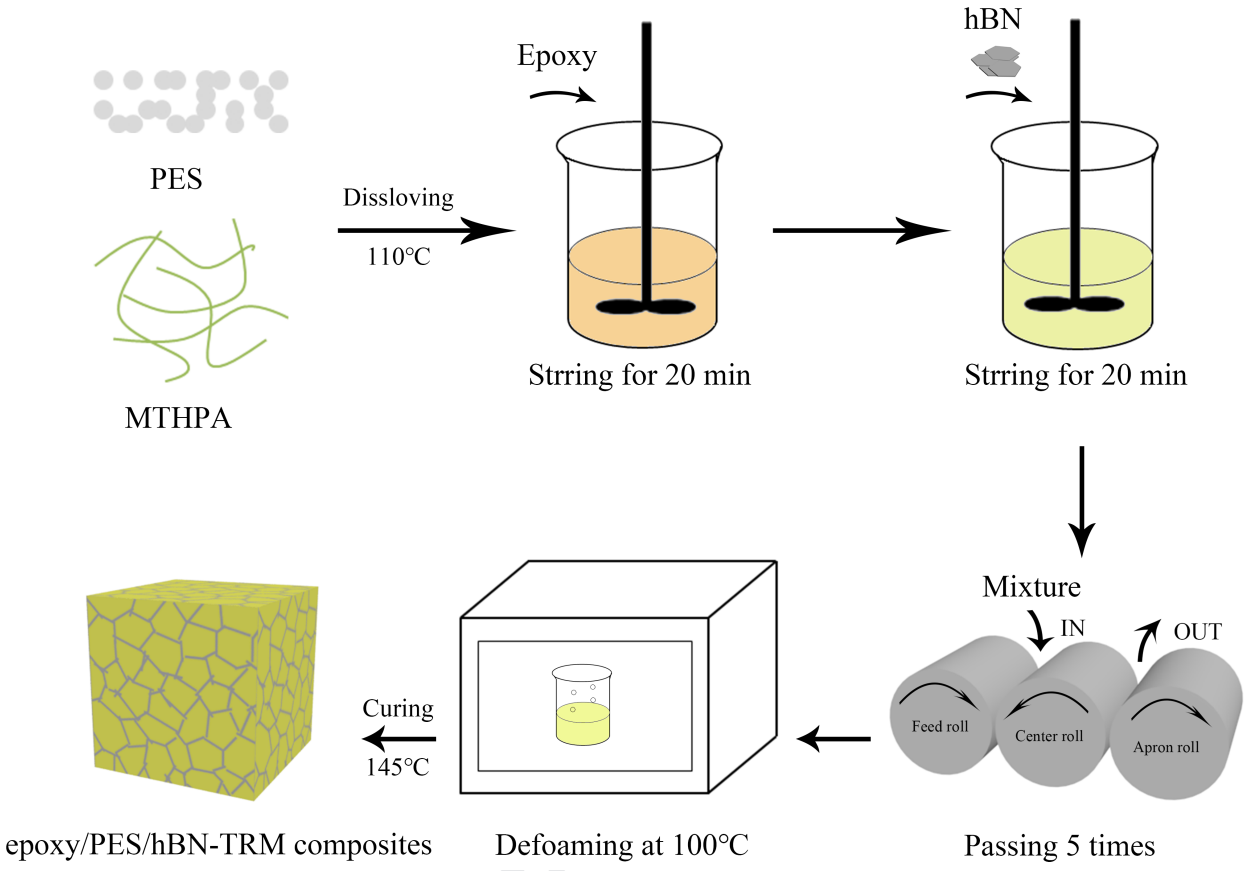
PES
MTHPA
Dissloving
110℃
Epoxy
Strring for 20 min
hBN
Strring for 20 min
Mixture
IN
OUT
Feed roll
Center roll
Apron roll
Passing 5 times
Defoaming at 100℃
Curing
145℃
epoxy/PES/hBN-TRM composites

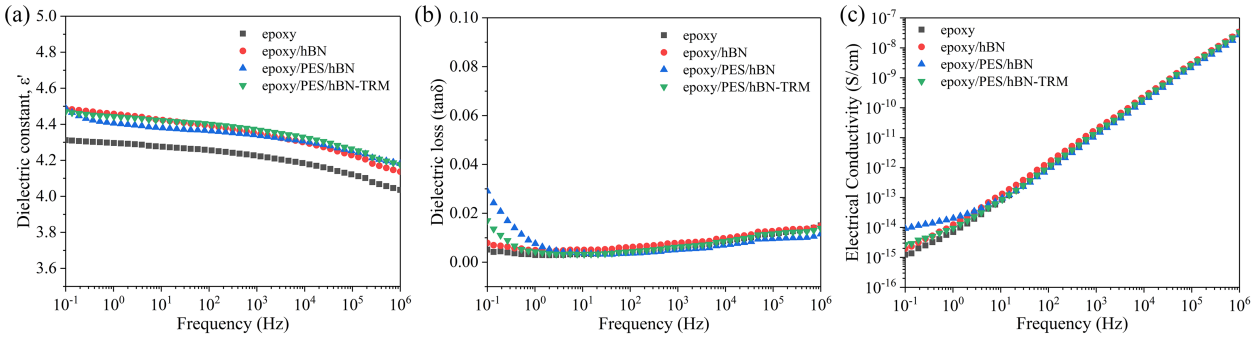

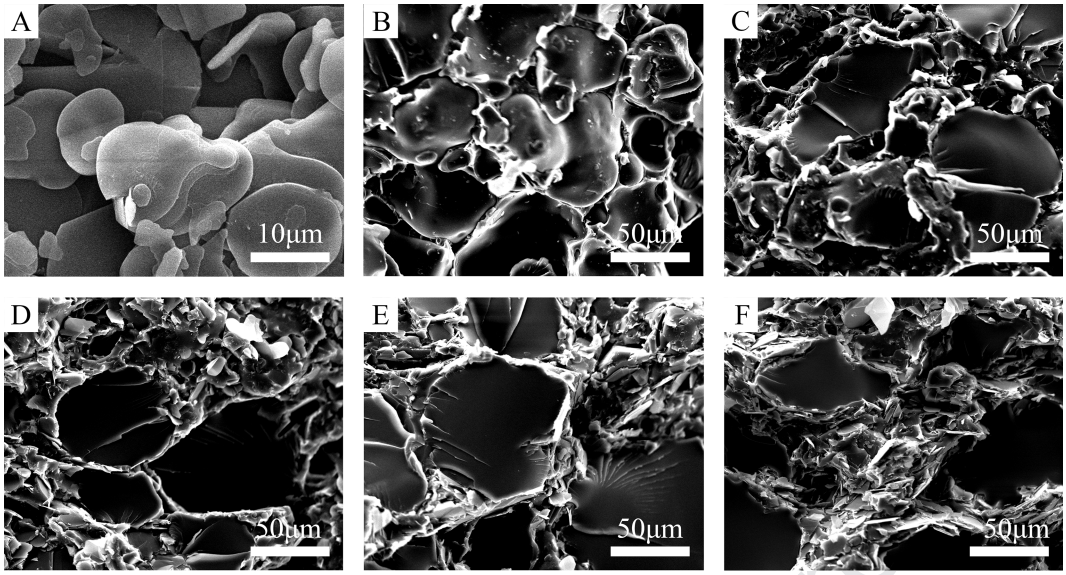

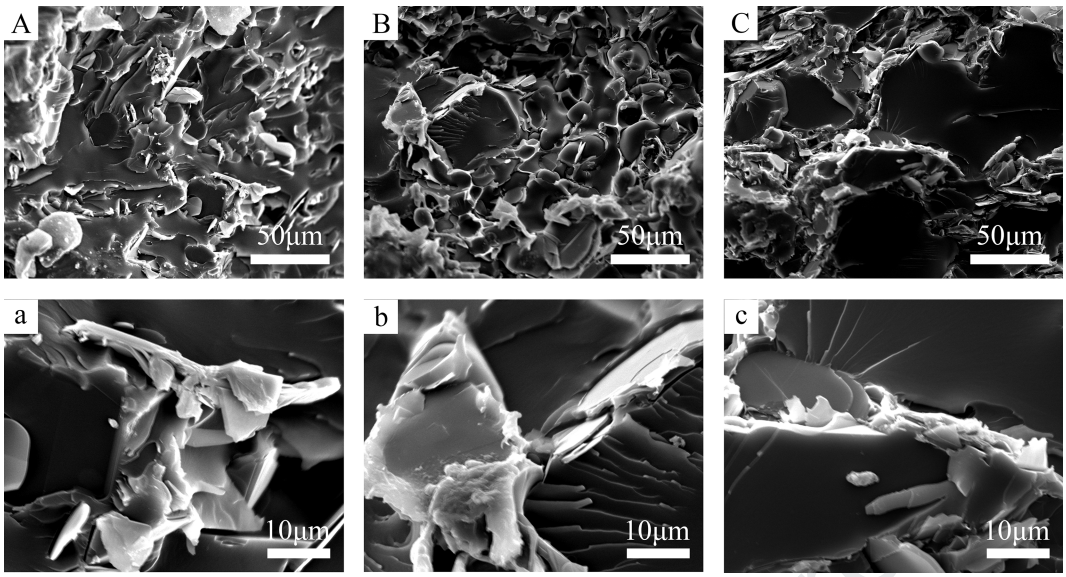

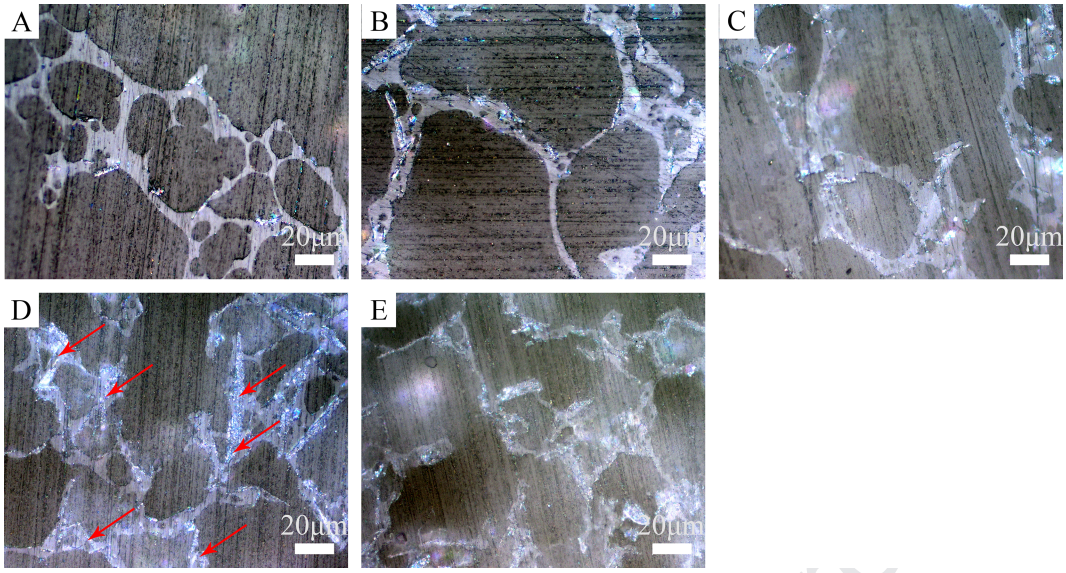

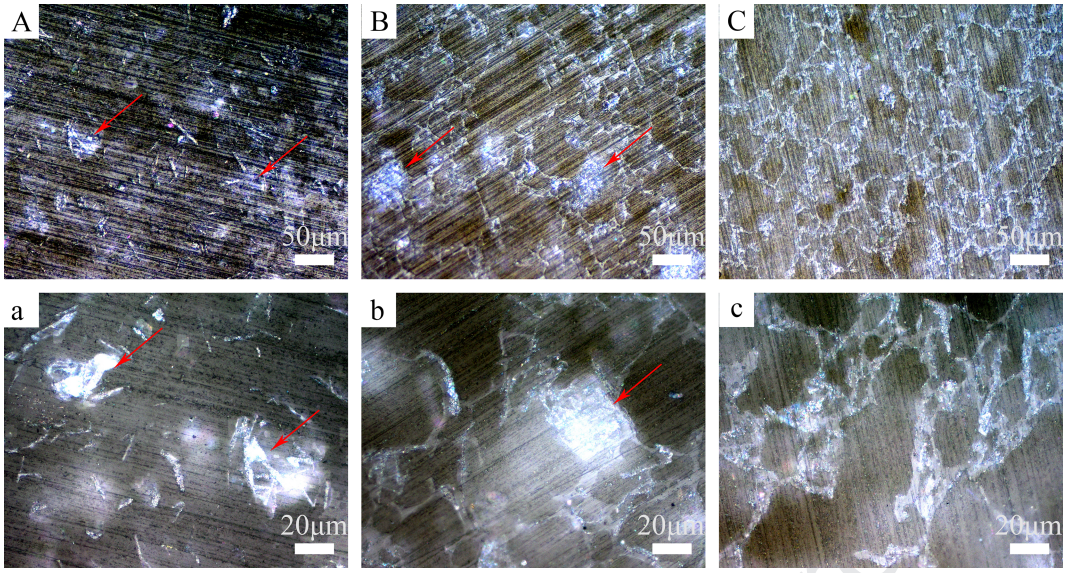

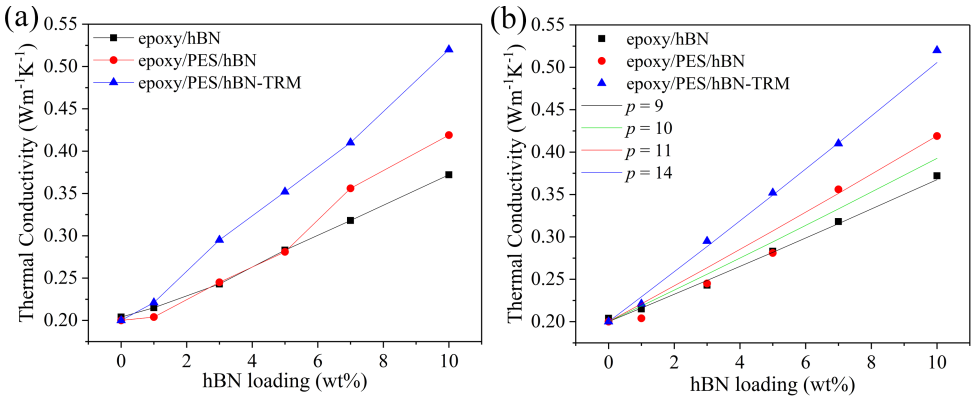

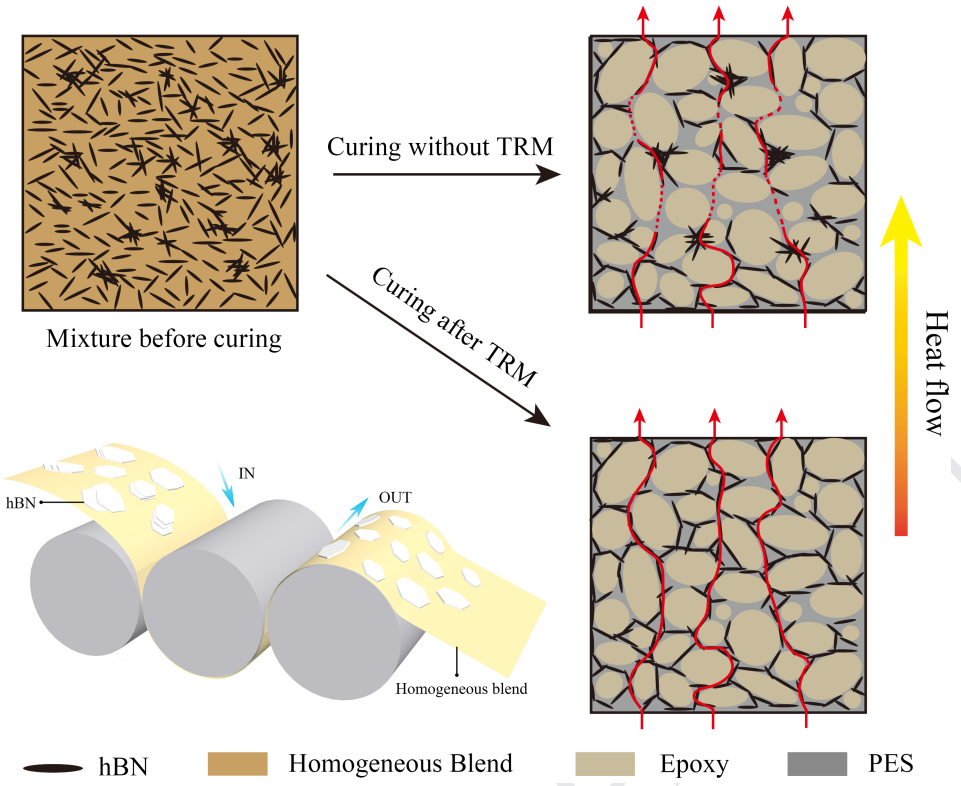

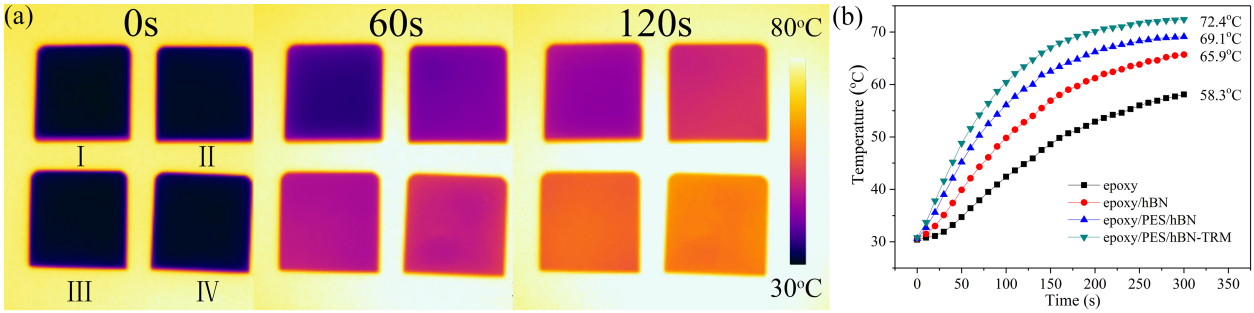

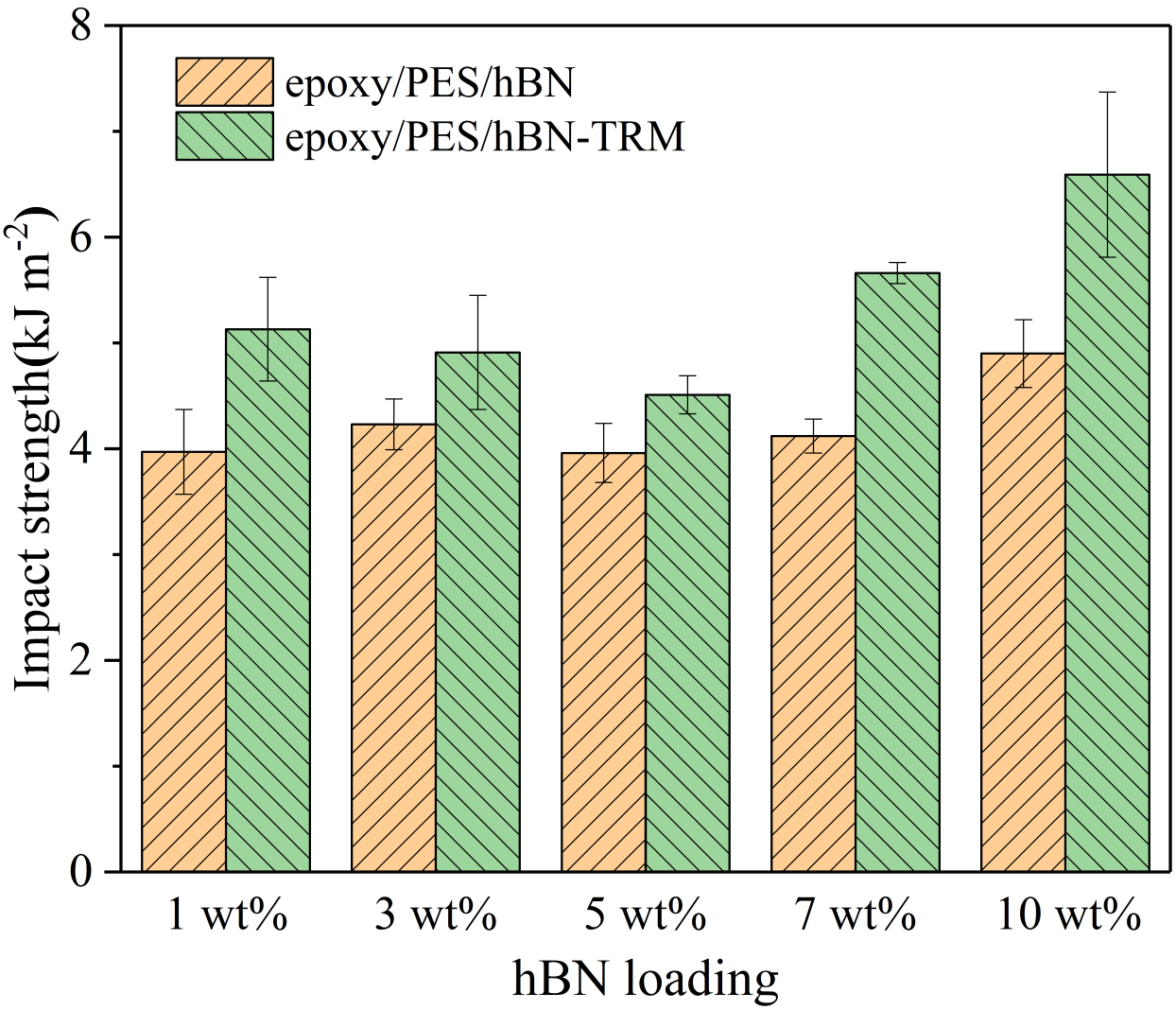
epoxy/PES/hBN
epoxy/PES/hBN-TRM
Impact strength(kJ m-2)
0
2
4
6
8
1 wt%
3 wt%
5 wt%
7 wt%
10 wt%
hBN loading

Author Statement:

Cong Gao: Conceptualization, Methodology, Validation, Formal analysis, Investigation, Data Curation, Writing-Original Draft, Writing-Review&Editing, Visualization.

Zihao Zhu: Methodology, Investigation, Data Curation, Visualization.

Yucai Shen: Conceptualization, Writing-Review&Editing, Supervision, Funding acquisition.

Tingwei Wang: Supervision.

Dong Xiang: Results discussion.

Declaration of interests

☒ The authors declare that they have no known competing financial interests or personal relationships that could have appeared to influence the work reported in this paper.

☐The authors declare the following financial interests/personal relationships which may be considered as potential competing interests: